Upsala J Med Sci 91: 37–43, 1986

Selective Properties of Trains of Real and Complex RF Micropulses in Slice-Selective Spin-Echo MRI

B. Jung,[1] A. Ericsson,[2] and A. Hemmingsson[2]

[1]*Department of Hospital Physics, University Hospital, Uppsala and* [2]*Department of Diagnostic Radiology, Uppsala University, Uppsala, Sweden*

ABSTRACT

The spin nutation properties of frequency selective (space selective in combination with a magnetic field gradient) trains of radiofrequency micropulses were studied in a numeric model. Two cases were considered, one simulating the 90 degrees excitation pulse in spin-echo MRI, the other the 180 degrees spin inversion pulse. Image reconstruction according to the 2-D Fourier transform technique requests that the effect of the 180 degree pulse is independent of the initial phase of the spin vector relative to the radiofrequency field. It was found that with a train of phase-stable radiofrequency micropulses with an envelope of the traditional 'sinc' type the result of the spin inversion pulse was depending on the initial phase whereas this was not the case for a train of phase-shifted (complex) micropulses. The complex train of radiofrequency micropulses also had better selective properties both for excitation and spin inversion than the real one.

INTRODUCTION

In magnetic resonance imaging (MRI) (1, 3, 5, 6, 8) 'selective excitation' stands for a space selective process in which a frequency-selective radiofrequency (rf) pulse is used to nutate the spins in a defined slice of the object under the influence of a linear magnetic field gradient. In the imaging technique applying the 2-D Fourier transform method (5), the rf pulse and magnetic field gradient sequence may be a 90 degrees excitation pulse combined with ZGRAD, defocusing and phase-encoding during XGRAD+YGRAD, and a 180 degrees pulse combined with ZGRAD where ZGRAD stands for a magnetic field gradient along the major field axis and XGRAD and YGRAD are mutually orthogonal gradients, orthogonal to this axis. A spin-echo recorded under XGRAD is then Fourier-transformed to yield the distribution of spins in the X-direction. A number of such sequences with proper Y-encoding (via a set of properly chosen gradients in the Y-direction, YGRAD) is recorded and a second Fourier transformation yields the two-dimensional

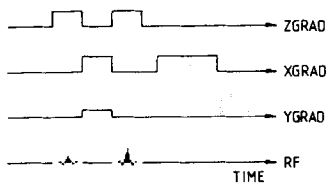

Fig. 1: Simplified schematic timing diagram of a spin-echo sequence in 2-D Fourier transform MRI.

spin-density in the slice (in this example in the XY-plane), defined by the two rf pulses applied under ZGRAD.

In such a process the second rf pulse (180 degrees) of necessity must handle, on an equal footing, elemental macroscopic magnetizations in the XY-plane, that have all possible phases in relation to the rf pulse.

When trying to simulate numerically the behaviour of a 2-D Fourier MRI system with respect to slice definition, object movements and spectrum of Larmor frequencies, an erratic behaviour with sudden narrow drops in spin-density sensitivity in the selected slice was found. This motivated a closer look on the phase-dependence of the space-selective processes.

In the first simulations a selective phase-stable rf pulse, proposed by Locher (7), was applied, in later ones the complex selective rf pulse suggested by Silver et al. (9, 10). Two situations were considered. In the first one the space selection and the resulting phase for nutation of a macroscopic magnetization in thermal equilibrium, were studied. This case simulates the 90 degrees excitation. In the second situation the space selection, the resulting magnetization in the XY-plane and the resulting phase for inversion of a macroscopic magnetization in the XY-plane were studied. In the latter case, simulating spin inversion, the calculations covered all initial phases.

METHOD

A simplified timing diagram of a spin-echo sequence is given in Fig. 1. The rf pulses were considered to be composed of 256 micropulses of suitably selected strengths but of constant amplitude and of constant phase, with respect to an assumed external clock, during their time period. They were applied in combination with the magnetic field gradient ZGRAD. The following XGRAD pulse defocuses the phases and is applied to correct for the phase development during the second XGRAD pulse, under which the echo is recorded. The YGRAD pulse, of variable amplitude, encodes the echo in the Y-direction.

The elements, BX and BY, of a complex rf vector were assigned values according

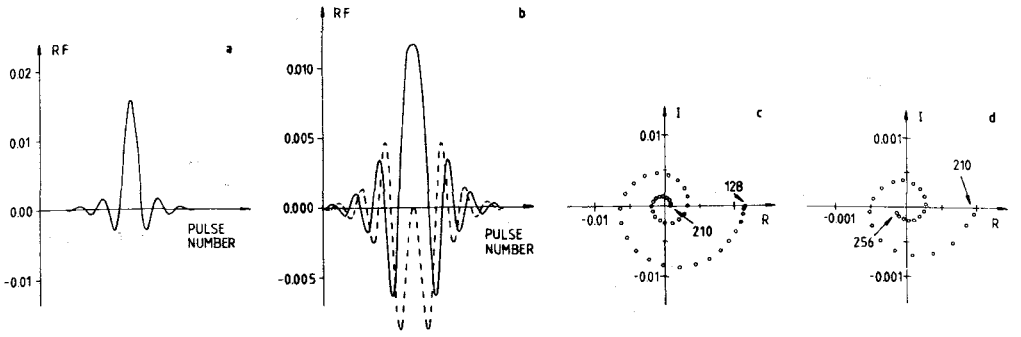

Fig. 2: Real pulse train (panel a) according to (7) and complex pulse train (panel b) according to (9, 10). The amplitudes are given in revolutions per micropulse period (Z=0) for a resulting nutation of 90 degrees. In the complex case this applies for the real component only. Both pulse trains are centered around micropulses 128 and 129. Panel c shows the phase diagram of the third quarter of the rf train and panel d the fourth quarter. Arrows indicate micropulse number.

to the formulae given by (7) and by (9, 10).

In the former, real, case this yielded

BX(I)=C*sinc(2*I/p)*exp(-I*I/(2*d*d)

BY(I)=0 (i.e. phase-stable)

where I=-128,128,1

p=128/4

d=95*p/24

sinc(J)=sin(PI*J)/(PI*J) and

PI=3.1416...

In the latter, complex, case the formulae were

BX(I)=C'*HELP1*cos(HELP2)

BY(I)=C'*HELP1*sin(HELP2)

where HELP1=2/(exp(I*INCR+5/256)+exp(-I*INCR+5/256))

HELP2=5*ln(HELP1) and

INCR=5/128;

The constants C and C' were varied in order to obtain various nutation angles.

The calculations were performed in a coordinate system rotating in the appropriate direction in synchronism with the Larmor frequency of the central disc of the slice (i.e. Z=0; no Z-gradient offset). The Z-axis was parallel to the main magnetic field, B0. The X-axis was orthogonal to the Z-axis and parallel to the BX of the rf field, and the Y-axis orthogonal to the other two axis and parallel to the BY of the rf field.

The numerical representation of all magnetic field vectors was scaled to give the precession angle during the time period of one micropulse. The resultant of the three components (in X-, Y- and Z-direction) was thus expressed as the

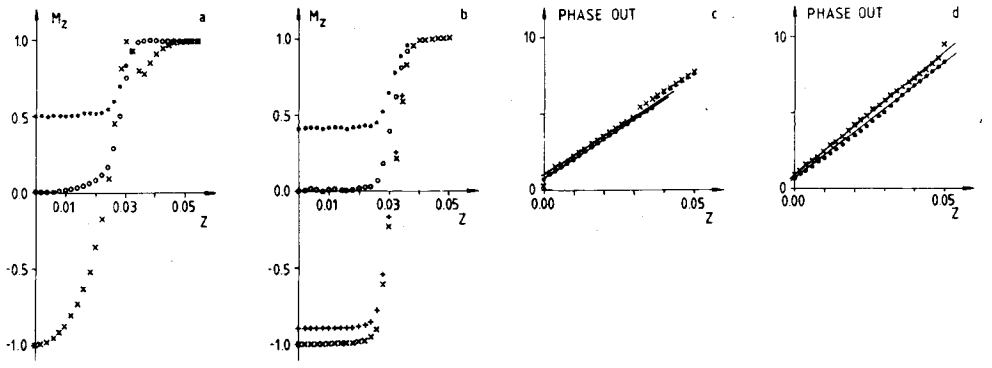

Fig. 3: Resulting macroscopic magnetizations in the Z-direction as a function of distance from slice centre after nutation of a (0,0,1) spin vector. Results with real pulse train in panel a and with complex pulse train in panel b. The nutation angles in panel a are 60 degrees (. . . .), 90 degrees (o o o o) and 180 degrees (x x x x), and the relative strengths of the complex train in panel b are 50 (. (. . . .), 70 (o o o o), 140 (+ + + +) and 200 (x x x x) (see the text for units). Panel c shows the resulting phase after nutation with the real pulse train as a function of distance from slice centre and the corresponding results with the complex pulse train is displayed in panel d. Nutation angles are in panel c 60 degrees (. . . .) and 180 degrees (x x x x) and in panel d the pulse strengths are 50 (. . . .) and 200 (x x x x). Nutation angles or pulse strengths between those given in panels c and d yield results in between the two curves in the digrams. The Z-distance is measured in Z-offset revolutions per micropulse period.

precession angle during the time period of one micropulse. The simulation procedure was then merely to multiply the magnetization vector, currently present, with the appropriate rotation matrix and to repeat this procedure 256 times. The nutation of the central (i.e. Z=0) elemental magnetization, when subjected to the real component of a micropulse train, is regarded as the nominal flip angle of the pulse.

Two cases of initial macroscopic magnetization were considered. In the first one the initial magnetization was the one at thermal equilibrium, i.e. parallel to the main magnetic field (B0), in vector notation (0,0,1). In the other case the macroscopic magnetization vector was supposed to initially be nutated to the XY-plane, in vector notation (sin(v),cos(v),0). (The vector notation is (x,y,z) with x=component of the macroscopic magnetization in the X-direction etc. and v=phase angle relative to the X-axis in the XY-plane immediately before the first micropulse of the simulated rf pulse train.)

Relaxation processes were ignored in the simulations which were performed on a PDP 11/40 computer with programs written in Fortran IV. Source codes are available on request.

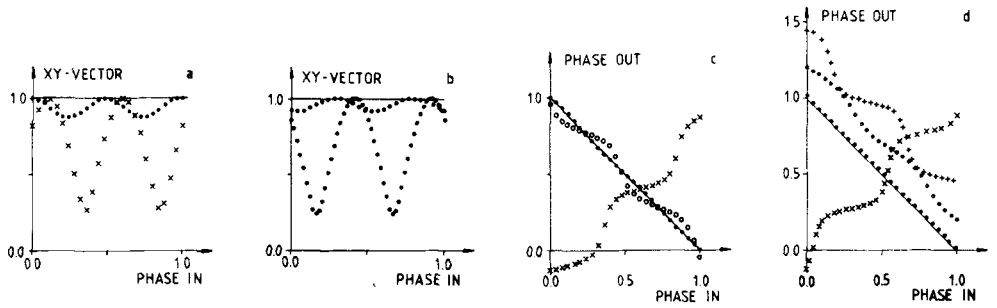

Fig. 4: Macroscopic magnetizations in the XY-plane as a function of initial phase after inversion of (sin(v),cos(v),0) spin vectors in the XY-plane. Results with real pulse train in panel a and with complex pulse train in panel b. Z=0 (central plane of the slice, ---------), Z=0.01 (panel a) and Z=0.025 (panel b) (. . . .), Z=0.025 (panel a) and Z=0.030 (panel b) (o o o o). The resulting phases of the macroscopic magnetizations as a function of initial phase after the same inversion is shown in panel c for the real pulse train and in panel d for the complex pulse train. Z=0 (central plane of the slice, --------), Z=0.010 in panel c and Z=0.025 in panel d (. . . .), Z=0.020 in panel c and Z=0.028 in panel d (o o o o), Z=0.025 in panel c and Z=0.032 in panel d (x x x x). In panel d Z=0.030 (+ + + +). All phases are measured in revolutions and the Z-distance is given as Z-offset precession revolutions per micropulse period.

RESULTS

The rf pulse trains are illustrated in Fig. 2. The resulting macroscopic magnetization in the Z-direction after an rf pulse train applied to a (0,0,1) macroscopic magnetization vector is given in Fig. 3 as a function of distance from the central plane (Z=0). Distance is measured as precession revolutions in the rotating coordinate system. For symmetry reasons only half of the selected slice is given in the illustration. The resulting phase after this procedure is also given in Fig. 3.

The macroscopic magnetization remaining in the XY-plane after nutation of a (sin(v),cos(v),0) macroscopic magnetization is given in Fig. 4 as a function of the initial phase v and the resulting phase after this procedure is also given in Fig. 4.

Only part of the results of the calculations are displayed in the figures.

DISCUSSION

The space selectivity of both pulse trains is rather good for 90 degrees pulses as illustrated in Figs. 3 and 4. The complex pulse train yields a somewhat more uniform magnetization along the Z-axis than does the real one. This effect is accentuated when the strengths of the pulse trains are increased to approach a nutation angle of 180 degrees. The mysterious property of the complex train

to approach 180 degrees inversion asymptotically for high pulse strengths was noted by (9, 10) and is evident in Fig. 3b.

For both types of 90 degrees pulse trains the resulting phase was almost linearly depending on position (Fig. 3c and d). As stated earlier (7, 9, 10) this seems to be a prerequisite for proper refocusing of the spins before the recording of the echo. The breaks in the linear functions occur well outside the space-selective regions.

The effect of the spin-inversion pulse trains is evidently depending on the initial phase (Fig. 4). This effect is, however, not very accentuated for the complex train until very close to the slice border. For the real pulse train the effect occurs closer to Z=0, and, in fact, Z=0.025 in Fig. 4a represents a case when a minimum in the XY-vector has already occurred at a smaller Z value.

Also the resulting spin phase is linearly depending on the incoming phase up to very close to the slice border for the complex rf train, whereas the real train gives distorsions rather close to the slice centre (Fig. 4b and c). This distorsion results in a bunching of the resulting phases around two preferred values. It is believed that this bunching may seriously affect the performance of the imaging system.

In simulations with other phase-stable pulse trains, not further detailed here, the bunching of phases was found to be associated with the occurrence of zeroes for some initial phases in the macroscopic magnetization in the XY-plane after inversion. An inverse proportionality of resulting phase on initial phase was found for Z values larger than the smallest one giving a zero (for some initial phases) in the resulting XY-vector. Such a behaviour is indicated in Figs. 3 and 4.

It thus seems difficult to have a good selective spin inversion in an MRI system provided the rf pulse is restricted to be real (phase-stable). Simulation experiments by (2, 4) support this statement. Unreported results obtained by us strengthens this conclusion since it was invariably found that spin bunching and low inversion efficiency occurred before the borders of the selected slice.

On the other hand a first trial with a train of complex rf micropulses gave a result free of most of the short-comings of the real pulse train. A complex rf pulse would add to the complexity of an MRI system but there should be no absolute technical obstacles to such a solution.

ACKNOWLEDGEMENT

Supported by grant from the Swedish Medical Research Council, proj. no. K84-17X-6676-02A.

REFERENCES

1. Damadian, R.: Apparatus and method for detecting cancer in tissue. US Pat. 3.789.832, filed March 17, 1972.
2. Frahm, J. & Hänicke, W.: Comparative study of pulse sequences for selective excitation in NMR imaging. J Magn Reson 60:320-332, 1984.
3. Hinshaw, W.S.: Spin mapping: the application of moving gradients to NMR. Phys Lett 48A:87-89, 1974.
4. Joseph, P.M., Axel, L. & O'Donnel, M.: Potential problems with selective pulses in NMR imaging systems. Med Phys 11:772-777, 1984.
5. Kumar, A., Welti, D. & Ernst, R.: NMR Fourier zeugmatography. J Magn Reson 18:69-83, 1975.
6. Lauterbur, P.C.: Image formation by induced local interactions: examples employing nuclear magnetic resonance. Nature 242:190-191, 1973.
7. Locher, P.R.: Computer simulation of selective excitation in n.m.r. imaging. Phil Trans R Soc Lond B289:537-542, 1980.
8. Mansfield, P. & Grannel, P.K.: NMR 'diffraction' in solids? J Phys Soc C: Solid State Phys 6:L422, 1973.
9. Silver, M.S., Joseph, R.I., Chen, C.-N., Sank, V.J. & Hoult, D.I.: Selective population inversion in NMR. Nature 310:681-683, 1984.
10. Silver, M.S., Joseph, R.I. & Hoult, D.I.: Highly selective pi/2 and pi pulse generation. J Magn Reson 59:347-351, 1984.